

Modeling and Simulation of a Tethered Harpoon for Comet Sampling

Marco B. Quadrelli*

This paper describes the development of a dynamic model and simulation results of a tethered harpoon for comet sampling. This model and simulation was done in order to carry out an initial sensitivity analysis for key design parameters of the tethered system. The harpoon would contain a canister which would collect a sample of soil from a cometary surface. Both a spring ejected canister and a tethered canister are considered. To arrive in close proximity of the spacecraft at the end of its trajectory so it could be captured, the free-flying canister would need to be ejected at the right time and with the proper impulse, while the tethered canister must be recovered by properly retrieving the tether at a rate that would avoid an excessive amplitude of oscillatory behavior during the retrieval. The paper describes the model of the tether dynamics and harpoon penetration physics. The simulations indicate that, without the tether, the canister would still reach the spacecraft for collection, that the tether retrieval of the canister would be achievable with reasonable fuel consumption, and that the canister amplitude upon retrieval would be insensitive to variations in vertical velocity dispersion.

I. Introduction

NASA is interested in designing a spacecraft capable of visiting a Comet, performing experiments, and then returning safely. Certain periods of this concept would require the spacecraft to remain stationary relative to the NEO. Such situations would require a harpooning mechanism that is compact, easy to deploy and upon mission completion, easily removed. The design philosophy used in the concept relies on the simulation capability of a multibody dynamics physics engine. On Earth it is difficult to create low gravity conditions and testing in low gravity environments, whether artificial or in space is costly and therefore not feasible. Therefore simulation is ideally suited to analyze the problem at hand.

The New Frontiers Comet Surface Sample Return (CSSR) concept is one of several potential missions to small primitive bodies. There have been prior cometary missions beginning with the European Space Agency (ESA) Giotto (fast flyby) and continuing with ESAs Rosetta mission, which will rendezvous with a comet and place a lander on it in 2015. Many of these new missions would require technologies such as Touch and Go (TAG), a type of autonomous rendezvous and docking *GN&C* system that could make close, controlled approaches and gentle contact with the rotating surface of the body, or different types of penetration systems such as harpoons, darts, or drilling end-effectors. Since ground testing of systems operating in microgravity is extremely costly, innovative approaches for integrated modeling and simulation of proximity operations will be needed to test system performance. Similar to the Mars Sample Return (MSR) concept, CSSR would require advances in the areas of sampling and sample handling, efficient operation methodologies, precise global localization, and advanced options for surface mobility in the cometary microgravity environments. Figure 1 depicts the mission scenario. Figure 2 shows the sequential steps of approach and departure from the comet (courtesy of Steve Broschart, JPL).

Utilizing a rover-mounted harpoon to collect samples from Mars cliffs and a balloon-mounted harpoon to sample the surface of Titan has been proposed.³ Other concepts are described in,^{16,17} Goddard Space Flight Center (GSFC) has proposed using a harpoon sampler for comet sampling.¹¹ The Hayabusa mission fired a projectile into the surface to dislodge surface material, which was captured.²⁸ In situ missions prepare and transfer samples to science instruments as implemented for the ESA RoLand/Philae (Rosetta) mission.⁸

*marco.b.quadrelli@jpl.nasa.gov, Mobility and Robotic Systems Section, Autonomous Systems Division, Jet Propulsion Laboratory, California Institute of Technology, 4800 Oak Grove Drive, Pasadena, CA 91109, senior AIAA member

The Sampler, Drill and Distribution System (SD2) is part of the Rosetta mission and is designed to collect 1 to 40 mm^3 of sample from a comet at a maximum depth of 230 mm.⁷ In,²⁷¹⁸ and¹⁹ tethers were proposed to retrieve a canister from a cometary surface.

In this paper, we leverage recent work on modeling and simulation of harpooning processes²¹ for the harpoon-soil interaction dynamics.

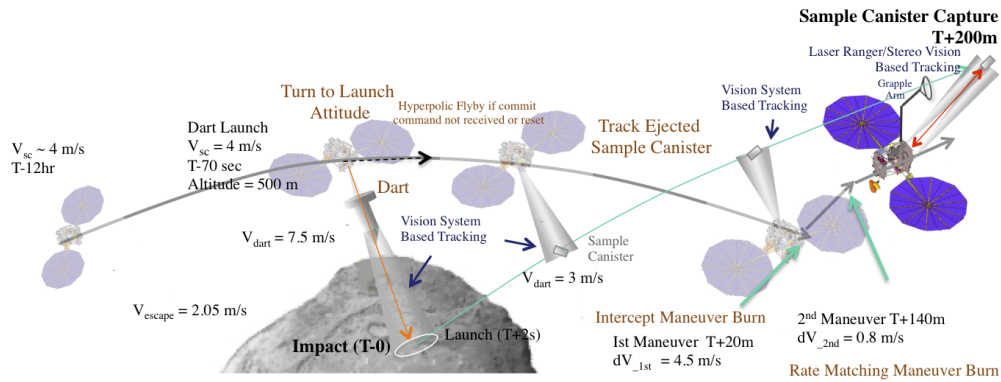


Figure 1. Mission Scenario

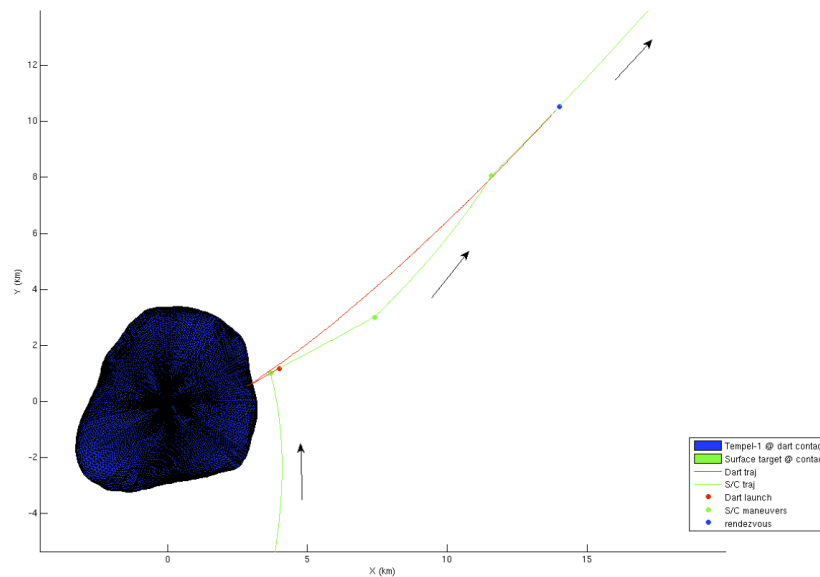


Figure 2. Steps of approach and departure from comet (courtesy of Steve Broschart, JPL)

II. Mission Concept

The mission concept involves several phases:

- Deployment: Fire harpoon from 100m+ from spacecraft (S/C) (nominal option).
- Sampler Stabilization: Sampler would be stabilized during flight to surface via tension in tether.
- Sampling: Passive, square, drive tube sampler would impact, sample, close and eject sample canister.

- Retrieval: S/C would reel in tether while S/C thrusts, possibly with pendulum cancellation maneuver.
- Sample Measurement: Potentially compute from balance of forces given the spacecraft acceleration.
- Canister Capture: Pull back into chamber it was released from.
- Canister Transfer to SRC: S/C arm would grasp canister and transfer to SRC.

The benefits of this approach would primarily be: low mission risk and capability of providing desirable science data. In regards to risk, the spacecraft would stay far from comet, and would never be on collision trajectory with comet. It would rely on a passive sampler, with the canister retrieval constrained to tether. The canister capture would be straightforward, and the canister transfer back to the spacecraft would also be straightforward. In terms of the desirable science, this approach would allow for sampling subsurface to 10cm, maintaining stratigraphy, would allow multiple samples from different comet locations, and would minimize sample contamination.

Once the spacecraft points the sampler at the target, then the sampler would simply be released toward the sample target. The tether spool would be on the sampler, and would be pulled out with constant tension, although another design option for active tether tension control would have the spool on the spacecraft instead. The tether tension would stabilize the sampler during flight to surface. Since the spacecraft could be at a stand-off distance, the tether could be long.

It is assumed that a spacecraft would stand off from a cometary nucleus by hundreds or even thousands of meters, and fire a harpoon-type sample capture device into the comet. Based on initial considerations at the mission level, the harpoon would need to penetrate approximately 10 cm into the surface material, capturing a core tube full of approximately 500cc of surface material. It would need to retain this material in the core tube, and then eject the core tube at more than the comet's escape velocity (approximately 2 m/s) so that it could be captured by the S/C for insertion in an Earth return capsule. The cometary surface material is thought to have a density of approximately 0.3g/cc and a strength (both in shear and compression) of 10-100kPa. The canister swing angle would also be bounded to stay within camera field-of-view for visual tracking, especially in close distances, to a semitone angle of approximately 15 degrees.

For the launch phase, the important considerations at launch would be: a) the attitude and body rates of S/C and harpoon; b) the horizontal and lateral velocities induced by spring; c) the maximum harpoon acceleration level, and d) an adequate selection of likely impact site. Important considerations at ground penetration would be: a) harpoon attitude and body rates relative to ground; b) horizontal and lateral velocities cause dispersion; c) regolith cohesion and friction angle of regolith; d) penetration depth; e) max. acceleration; f) possible ricochet, and g) possible impact at site with unfavorable surface orientation. Important considerations at canister ejection would be: a) harpoon attitude and body rates relative to ground, and b) horizontal and lateral velocities cause dispersion.

Two cases are considered in this paper. In the first case, the canister would be retrieved from the emplaced harpoon via an ejection impulse. In the second case, the canister would be retrieved via a tether. Figure 12 (a) shows the model of the tethered retrieval. Figure 12 (b) depicts the various events that would take place during the tethered canister ejection. Figure 5 summarizes the various system parameters considered in this study.

The process of retrieving, collecting, and packaging a sample for a purpose such as sample return must be distinguished from the kind of manipulation used in an in situ mission. There is a clear distinction between sample acquisition, which relies on an end-effector to collect the sample, and sample caching, which involves the transfer and handling of the sample so that would be safely placed for subsequent analysis (either in situ, or for transfer back to the Earth). Figure 3 indicates how the principal *GN&C* functions would be integrated in a sample collection event. The yellow box denotes the functional areas relevant to this report, and the number of red dots indicates those areas requiring more technology development than others. Furthermore, there are significant differences between sampling on bodies with significant gravity and sampling on small bodies with little gravity. Amongst small bodies, there are differences between sampling comets and sampling asteroids. For instance, sampling of small bodies takes place in an environment where a) material cohesion and surface adhesion effects dominate particle interactions at small scales through Van der Waals forces, b) electrostatic forces are generally negligible except near terminator crossings where they can lead to significant dust transport, and c) micro-gravity and solar radiation dominate system behavior prior to end-effector soil engagement/harpoon penetration.

To provide context, the study approach is built upon an integrated set of physics-based models as illustrated in Figure 3. The focus of this paper is on the right side of this block diagram. The block diagram shows each element of the integrated model of spacecraft and end-effector dynamics,⁴ which includes the models of: the planning function, where the spacecraft trajectory and attitude are specified; the vehicle attitude and orbital dynamics; the vehicle GNC functions, including orbital and attitude estimator and navigation filters; the deployable manipulator dynamics and hinge actuation; the end-effector, harpooning, or in-situ sampling device dynamics and actuation; the Small Body shape, orbital dynamics, and polyhedral gravity models; the communication, power, and lighting geometric analysis; the multi-scale properties of the surface regolith; and the interaction of the end-effector, harpooning, or in-situ sampling device with the surface regolith. The block diagram includes feedback loops to the spacecraft controller from the hinge states of a deployed robotic manipulator, the end effector states, and the amount of mass collected, assuming all these states are known. If not known, they can possibly be estimated. The reason for including these additional functions is that sensing these states are all possibilities in a scenario where an algorithm is needed to monitor the duration of the sample event (dwell time), and a change in each one of these states can be used as a trigger to terminate the event. Utilizing force sensing and active compliance during sample collection has also been proposed in,^{20,21} and is an example of close integration between the *GN&C* functions and the sample collection dynamics. This solution would allow the sampler to contact and penetrate the surface while the spacecraft is far away from it, and would dramatically increase the likelihood of successful sample collection and return of pristine samples to Earth, with great benefit to planetary science. Small body sampling from a long stand-off boom not only poses lower risk to the spacecraft, but would allow for longer sampling durations and depths than possible with existing articulated arms and booms in closed proximity of the surface, and for sampling multiple times at multiple locations for a fixed spacecraft position.

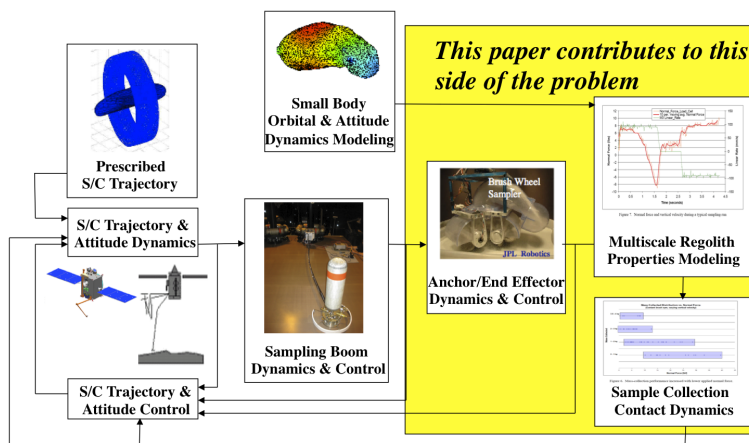


Figure 3. Comet GNC block diagram.

An important element in the understanding of the harpooning penetration process is the physics of the regolith, which is described next.

III. Modeling of System Dynamics

The modeling approach described in this section presents several challenges. First, a complex system needs to be modeled which simulates a complex mission phase: approach to the comet, release of the harpoon, harpoon emplacement on the ground, release of the canister from the harpoon, and recovery of the canister by the spacecraft. We approach these challenges by using a multi-body dynamics modeling approach, in which all bodies (spacecraft, harpoon, canister) are initially kinematically locked, then released and unlocked when an impulse is applied. We also emphasize the interaction between the harpoon and the soil model, as this interaction drives the initial conditions for the next phase, i.e. the ejection or tethered retrieval back to the spacecraft.

Therefore, two systems have been considered that deal with this complexity.

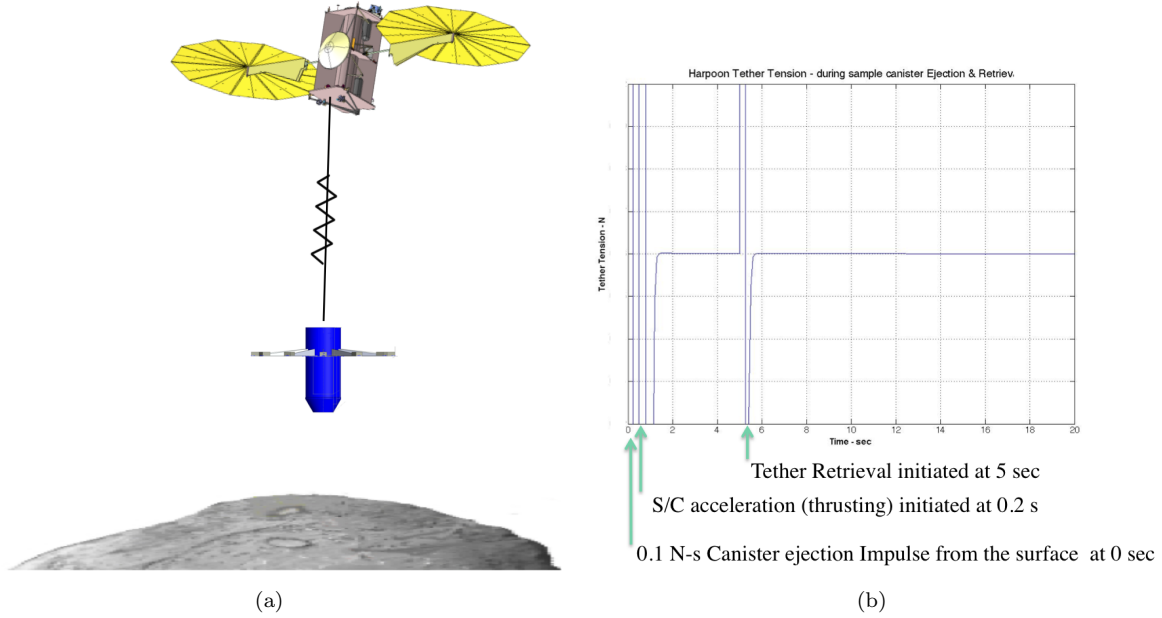


Figure 4. (a) Model of tethered harpoon, and (b) Event Timeline.

First, a three-dimensional model of the system composed of the spacecraft, the harpoon, and the canister inside the harpoon has been considered. Second, a two-dimensional model of the tethered canister being retrieved by the spacecraft has been considered. A two-dimensional model for the tethered system was chosen to focus on the main issue of bringing the canister within reach of the spacecraft, rather than focusing unnecessarily on complex tether dynamics. The two systems have the initial phase in common, i.e. the harpoon ejection and penetration phase, since to first order the high separation impulse of the harpoon from the spacecraft makes the tether tension much smaller than the harpoon inertia forces.

A. Three-dimensional dynamics of spacecraft-harpoon-canister system

The spacecraft, harpoon, and canister are assumed to be rigid bodies. The three bodies are initially rigidly connected. Upon ejection, the harpoon-canister system would first be released, while the spacecraft continues along its trajectory. Once collision with the ground has been made, the harpoon-canister system would be allowed to penetrate into the ground, so that a sufficient amount of sample could be collected into the canister. The canister body would also be kinematically released from the harpoon body. After a pre-specified time (1 second), the canister body would be spring ejected from the harpoon with a 2 kN force for 10 milliseconds, upwards towards the spacecraft. To allow for misalignments both at the harpoon-canister ejection from the spacecraft and at canister ejection from the ground, these ejection events would take place with both a force and a torque impulse. The canister would then travel towards the spacecraft, where a conical receiving funnel would collect it and secure it for return to the Earth. Important considerations at canister ejection are that the canister attitude and body rates relative to ground must be bounded to avoid tumbling, and that the horizontal and lateral velocity dispersions upon ejection could cause the canister to miss the rendezvous with the spacecraft.

The system Lagrangean is $\mathcal{L}(\eta, \dot{\eta}, t) = \mathcal{T}(\eta, \dot{\eta}) + \mathcal{U}(\eta, t)$, $\mathcal{T}(\eta, \dot{\eta})$ is the kinetic energy of \mathcal{S} and $\mathcal{U}(\eta, t)$ the potential energy of \mathcal{S} , η and $\dot{\eta}$ are the vectors of generalized coordinates and speeds, and F is the vector of generalized forces. The vectors η , $\dot{\eta}$, and F are defined as follows: $\eta = (\mathbf{r}_i, \mathbf{q}_i)$, $\dot{\eta} = (\dot{\mathbf{r}}_i, \omega_i)$, and $F = (\mathbf{f}_g + \mathbf{f}_i, \tau_i)$. The vectors \mathbf{f}_i and τ_i include external perturbation and control forces, and \mathbf{f}_g represents the gravitational force $-\mu m_i \frac{\mathbf{r}_i}{|\mathbf{r}_i|^3}$, the comet outgassing force, the solar pressure force, and the comet dust ejection force, described below. The virtual displacements $\delta \mathbf{r}_i$ and virtual rotations θ_{δ_i} are kinematically admissible as they satisfy any constraint equation imposed on body i , namely if $\Phi_{\mathbf{r}_i} \cdot \delta \mathbf{r}_i + \Phi_{\theta_i} \cdot \theta_{\delta_i} = 0$, where $\Phi = [\Phi_{\mathbf{r}_i}, \Phi_{\theta_i}]$ represents the Jacobian of a certain algebraic equation $\Psi = \Psi(\eta, \dot{\eta}, t) = \mathbf{0}$. Therefore, there

Parameter	Description	Values
M_sc	Spacecraft Mass	2500 kg
l(0)	Launch height (m)	100
M_h	Canister Mass	2 kg
Th	S/C Thrust	[10, 20, 30] N
Vh	S/C horizontal Vel.	@t0= [1, 5, 10] cm/s in +x
Vv	S/C vertical Vel.	@t0= [1, 2, 3] m/s in +y
K	Tether Stiffness	1.1343e+04 N/strain
C	Tether viscoelastic damping	49.24 Ns/strain
dl/dt	Tether retrieval rate	[10, 20, 30] cm/s

Figure 5. Parameter table

exists a vector of Lagrange multipliers λ such that, for arbitrary admissible $\delta \mathbf{r}_i$ and $\theta_{\delta i}$, the new equations of motion for body i become:

$$m_i \ddot{\mathbf{r}}_i = -\mu m_i \frac{\mathbf{r}_i}{|\mathbf{r}_i|^3} + \mathbf{f}_i + \Phi_{\mathbf{r}_i}^T \lambda \quad (1)$$

$$\mathbf{J}_i \dot{\omega}_i + \tilde{\omega}_i \mathbf{J}_i \omega_i = \tau_i + \Phi_{\theta_i}^T \lambda \quad (2)$$

The equations of motion can now be written in matrix form as:

$$\begin{bmatrix} \mathbf{M} & \Phi^T \\ \Phi & \mathbf{0} \end{bmatrix} \begin{pmatrix} \ddot{\eta} \\ \lambda \end{pmatrix} = \begin{pmatrix} \mathbf{g} \\ \mathbf{0} \end{pmatrix} \quad (3)$$

where

$$\begin{pmatrix} \ddot{\eta} \\ \lambda \end{pmatrix} = \begin{pmatrix} \ddot{\mathbf{r}}_i \\ \dot{\omega}_i \\ \ddot{\mathbf{r}}_j \\ \dot{\omega}_j \\ \lambda_r \\ \lambda_\theta \end{pmatrix} \quad (4)$$

$$\begin{pmatrix} \mathbf{g} \\ \Gamma \end{pmatrix} = \begin{pmatrix} \mathbf{f}_i - \mu m_i \frac{\mathbf{r}_i}{|\mathbf{r}_i|^3} \\ \tau_i - \tilde{\omega}_i \mathbf{J}_i \omega_i \\ \mathbf{f}_j - \mu m_j \frac{\mathbf{r}_j}{|\mathbf{r}_j|^3} \\ \tau_j - \tilde{\omega}_j \mathbf{J}_j \omega_j \\ 0 \end{pmatrix} \quad (5)$$

$$\mathbf{M} = \begin{bmatrix} m_i \mathbf{1}_3 & 0 & \mathbf{0} \\ 0 & \mathbf{J}_i & \mathbf{0} \\ \mathbf{0} & \mathbf{0} & m_j \mathbf{1}_3 & 0 \\ \mathbf{0} & \mathbf{0} & 0 & \mathbf{J}_j \end{bmatrix} \quad (6)$$

The constraints used in the spacecraft-harpoon-canister problem are essentially ground constraints (the harpoon locked to the ground at the end of penetration), and lock-release constraints before the various separation events take place.

B. Two-dimensional dynamics of canister tethered retrieval

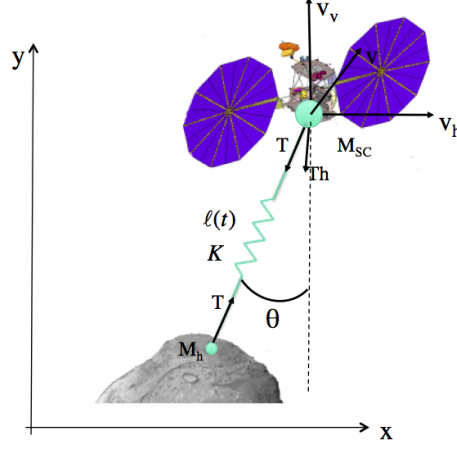


Figure 6. Model of system with tether.

The system model is assumed to be two-dimensional. Figure 6 depicts the geometry of the model used for this case. The horizontal and vertical components of velocity are to be considered as velocity dispersions, i.e., sources of error. T is the tether tension, Th is the spacecraft fly-away thrust, K is the viscoelastic tether impedance, and θ is the tether swing angle, which increases during retrieval, as tether retrieval is an unstable dynamic event.¹⁵ The spacecraft and harpoon are assumed to be rigid bodies connected by one viscoelastic spring. The equations of motion for the spacecraft and harpoon are:

$$\begin{pmatrix} \ddot{x}_{sc} \\ \ddot{y}_{sc} \\ \ddot{\theta}_{sc} \end{pmatrix} = \begin{pmatrix} m_{sc} & 0 & 0 \\ 0 & m_{sc} & 0 \\ 0 & 0 & J_{sc} \end{pmatrix} \cdot \begin{pmatrix} fsc_x - T_x + Fsc_x \\ fsc_y - T_y - m_{sc}g + Fsc_y \\ \tau_{sc} \end{pmatrix} \quad (7)$$

$$\begin{pmatrix} \ddot{x}_h \\ \ddot{y}_h \\ \ddot{\theta}_h \end{pmatrix} = \begin{pmatrix} m_h & 0 & 0 \\ 0 & m_h & 0 \\ 0 & 0 & J_h \end{pmatrix} \cdot \begin{pmatrix} fh_x + T_x + fGround_x \\ fh_y + T_y - m_h g + fGround_y \\ \tau_h \end{pmatrix} \quad (8)$$

where fsc and fh are the external forces on the spacecraft and harpoon, respectively, Fsc is the ascent thrust on the spacecraft, τ_{sc} and τ_{fh} are the external torques on the spacecraft and harpoon due to the tether, respectively, and $fGround$ is the force exerted on the harpoon upon ground penetration. Given the rotation matrices:¹⁰

$$A_i = \begin{pmatrix} \cos\theta_i & -\sin\theta_i \\ \sin\theta_i & \cos\theta_i \end{pmatrix} \quad (9)$$

$$B_i = \begin{pmatrix} -\sin\theta_i & -\cos\theta_i \\ \cos\theta_i & -\sin\theta_i \end{pmatrix} \quad (10)$$

the generalized forces on the spacecraft and harpoon body due to the tether are:

$$Q_{sc} = \frac{T}{L} \begin{pmatrix} d_{ij} \\ d_{ij}^T B_{sc} s_{sc} \end{pmatrix} \quad (11)$$

$$Q_h = -\frac{T}{L} \begin{pmatrix} d_{ij} \\ d_{ij}^T B_h s_h \end{pmatrix} \quad (12)$$

where $d_{ij} = r_j + A_j s_j - r_i - A_i s_i$, s_i is the location of the tether attachment point in the i -th body frame, and the tether tension is given by $T = k\varepsilon + c\dot{\varepsilon}$, where $\varepsilon = (L(t) - L_0)/L_0$ is the tether strain and $\dot{\varepsilon} = [(\dot{L}(t) - \dot{L}_0)L(t) - (L(t) - L_0)\dot{L}(t)]/L_0^2$ is the tether strain rate.

In the case of the canister being spring-ejected from the harpoon in the direction of the spacecraft, i.e. no tether assisted retrieval, the equations of motion of the canister become;

$$\begin{pmatrix} \ddot{x}_{co} \\ \ddot{y}_{co} \\ \ddot{\theta}_{co} \end{pmatrix} = \begin{pmatrix} m_{co} & 0 & 0 \\ 0 & m_{co} & 0 \\ 0 & 0 & J_{co} \end{pmatrix} \cdot \begin{pmatrix} f_{co_x} + F_{co_x} \\ f_{co_y} - m_{co}g + F_{co_y} \\ \tau_{sc} \end{pmatrix} \quad (13)$$

The algorithms used in the tether retrieval and canister collection events are shown in Figure 7. Some relevant ideas are also discussed in¹⁸ and¹⁹

<pre> Tether retrieval guidance: if (iRetrieve=1 & iPayloadGrabbed=0), if (TEA < 15 deg), $\dot{L}_0 = \text{retrievalRate}$, end if (TEA >= 15 deg), $L_0 = \text{retrievalRate}$; end end $L(t) = L_0 + \dot{L}_0(t - t_{\text{retrieve}})$ $\dot{L}(t) = \dot{L}_0$ </pre>	<pre> Canister capture logic: if (el<=elFinal & iPayloadGrabbed=0), $L(t) = L_0 + \dot{L}_0(t_{\text{canisterCollected}} - t_{\text{retrieve}})$ $\dot{L}(t) = 0$ canister collected and tether disconnected end </pre>
(a)	(b)

Figure 7. Tether retrieval guidance (a) and canister collection guidance (b).

C. Control Laws

The control laws applied to the spacecraft are of the feedback (proportional-derivative) plus feedforward type. The translation control that would actually be implemented on the spacecraft is of the form

$$\mathbf{f} = \mathbf{K}_p(\mathbf{s}_{Cmd} - \mathbf{s}_{Est}) + \mathbf{K}_v(\dot{\mathbf{s}}_{Cmd} - \dot{\mathbf{s}}_{Est}) + \mathbf{M}\ddot{\mathbf{s}}_{Cmd} \quad (14)$$

where \mathbf{s} represents the position vector of the center of mass, \mathbf{K}_p and \mathbf{K}_v are translation control gain matrices, \mathbf{M} is the spacecraft mass matrix, \mathbf{s}_{Est} and \mathbf{s}_{Cmd} represent the estimated and commanded translation state, respectively. The rotational control instead is of the following form

$$\tau = \mathbf{\Gamma}_p \lambda(\theta_{err}) + \mathbf{\Gamma}_v(\omega_{Cmd} - \omega_{Est}) + \mathbf{J}\ddot{\alpha}_{Cmd} \quad (15)$$

where $\mathbf{\Gamma}_p$ and $\mathbf{\Gamma}_v$ are rotational control gain matrices, \mathbf{J} is the spacecraft moment of inertia matrix, λ is the eigen-axis of rotation, and θ_{err} is the magnitude of rotation corresponding to the difference between the commanded and the estimated quaternions. A feedforward term is used to track a command defined up to an acceleration profile. The torques in eq.(15) are applied with a negative sign to the spacecraft reaction wheels.

IV. Modeling of Harpoon Interactions with the Ground and the Comet Environment

A. Harpoon penetration physics

Projectiles traveling through the ground do not always travel in a straight path. Under certain conditions, the trajectory will take on a curvilinear shape. This J-Hook phenomenon makes it difficult to determine the trajectory. Additionally, the entire harpoon would not stay in contact with the surrounding soil. This condition is known as Wake Separation. A stress would be exerted on the harpoon only where the soil is in

contact with the surface of the harpoon. Finally, there is Trajectory Direction Reversal. At some critical incidence angle a harpoon that would normally execute a J-Hook trajectory no longer travels back toward the surface, but dives away from the surface, driving the harpoon much deeper than expected. All of these issues make accurate prediction of a penetrator's trajectory very challenging. Large cometary bodies typically spin slowly and may have more strengthless material on the surface than small bodies, which tend to spin faster. For example: a buried circular disk penetrator has a vertical pullout capacity of about 68 times the weight of the soil in a cylinder above the disks surface area, for a soil friction angle $\phi = 40$ deg and a depth of burial 10 times the disk diameter. Therefore, for a 10 km radius asteroid with 2000 kg/m³ regolith, a vertical pull-out capacity of 300N requires the weight of 0.26 m³ of regolith, or a 32 cm diameter disk buried at a depth of 3.2 m. A cylindrical harpoon (pile) is an alternative choice, but still requires a diameter of 32 cm and a length of 7m for pullout capacities of 300N on 10 km radius asteroids, using the pile skin friction equations. In practice, there may be predominantly lateral loading on the harpoon, which complicates the analysis. It is likely that regolith harpoons would require significant burial depths and surface areas to be effective. With slow penetration methods (drill, melter), the attitude control system must be involved to stabilize the spacecraft. With fast penetration method (tethered spike, telescoping spike, multi-legged with tethered or telescoping spike), the attitude control system may not have to be involved. Early studies on penetration for the ST4/Champollion mission selected a 1 kg 1.9cm diameter truncated cone penetrator for penetration onto the surface on materials of strength up to 10 Mpa with a 45 degree impact angle within a reasonable velocity range (100-200 m/s) with a minimum pullout resistance of 450 N in any direction. Penetration deployment/retrieval issues: the harpoon may ricochet adversely on surface instead of solidly emplacing on ground. Drilling a harpoon requires a torque transfer to another object. PHILAEs landing gear uses ice screws and three landing legs with two pods in each, for example. Harpoons could be easily launched before landing. Spacecraft ACS (reaction wheels, not RCS) would probably need to be on during the penetration Phase to avoid vehicle stability problems. Some harpoon designs would allow them to be pulled out, others would not. Figure 8 and Figure 9 are taken from,⁵ and depicts the ranges of forces that would be expected in proximity of the surface of a comet. Figure 10, taken from,²³ summarizes typical behavior observed in penetration tests on different types of targets, indicating the possibility of ricochet of the projectile depending on the approach speed, direction, and surface material parameters.

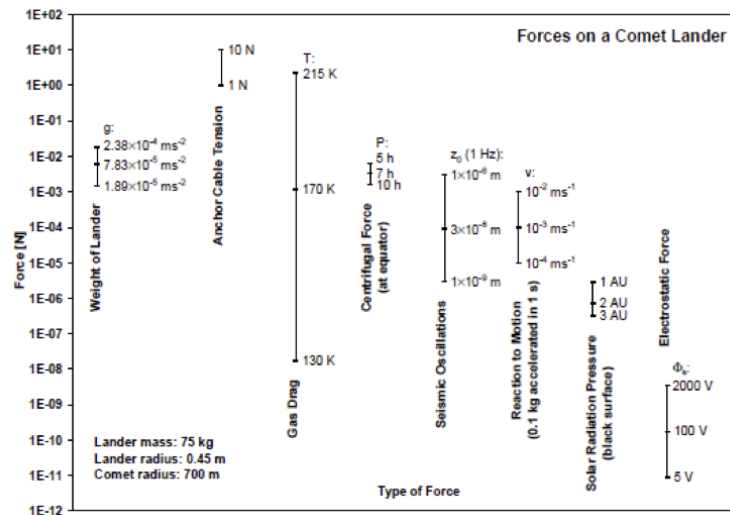


Figure 8. Forces On Comet Lander, taken from⁵

1. Regolith Modeling

In general, slow harpooning methods such as those based on drilling or melters would require the spacecraft Attitude Control System (ACS) to be involved for vehicle stabilization. Conversely, fast harpooning method such as those based on tethered spikes, telescoping spikes, and multi-legged with tethered or telescoping spikes would likely require less ACS involvement. Early studies on harpooning for the ST4/Champollion mission

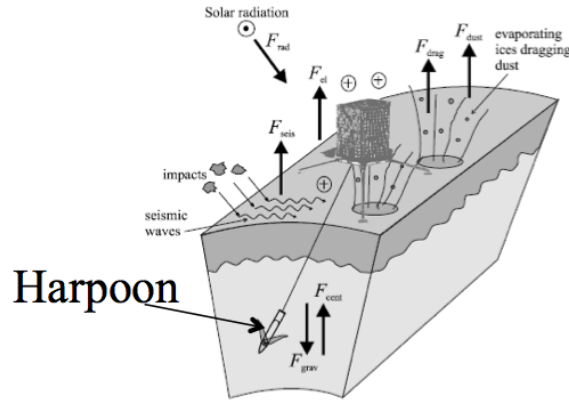


Figure 9. Environment around harpoon on Comet, taken from⁵

selected a 1 kg 1.9cm diameter truncated cone penetrator for harpooning onto the surface on materials of strength up to 10 Mpa with a 45 degree impact angle within a reasonable velocity range (100-200 m/s) with a minimum pullout resistance of 450 N in any direction. Several harpooning deployment/retrieval issues must be carefully considered that could impact the mission design. A harpoon may ricochet adversely on surface instead of solidly emplacing on ground. Also, drilling a helical harpoon requires a torque transfer to another object. PHILAEs landing gear uses ice screws and three landing legs with two pods in each, for example. Harpoons could be easily launched before landing. More than one harpoon would need to be deployed from the spacecraft to ensure static stability. Spacecraft ACS (reaction wheels, not RCS) would probably be needed to be on during the harpooning Phase to avoid slack cables and vehicle stability problems. Some harpoon designs would allow them to be pulled out, others would not.

Behavior of the regolith is likely governed by cohesion and surface adhesion effects that dominate particle interactions at small scales through van der Waals forces. Electrostatic forces are generally negligible except near terminator crossings where it can lead to significant dust transport. The micro-gravity and solar radiation dominate system behavior prior to soil engagement or penetration.

Soil mechanics experiments have known issues when it comes to testing samples of regolith in one-g. First, a reproducible preparation of a homogeneous soil sample is difficult to achieve. Second, a characterization of the soil properties in depth is difficult, since static parameters are typically measured at the surface. Third, under 1-g load, according to soil theory, the compressive strength in depth is significantly influenced by overburden terms, i.e. the effective strength/resistance increase with depth. The soil shear stress can be modeled as

$$\sigma_c = c + p \tan(\phi_f) \quad (16)$$

i.e. , the Mohr-Coulomb limit soil bearing capacity theory, where ϕ_f , is known as the friction angle (or internal-angle-of-friction), p is normal pressure, and the zero normal-stress intercept, c , is known as the cohesion (or cohesive strength, i.e. shear stress at $p=0$) of the soil. For typical regolith simulant, the cohesion is 40 Pa at loosely packed conditions and increases to 10 kPa at 100 relative density. The friction angle also increases monotonically from 25 deg to 60 deg. The Rosetta Lander design takes advantage of this effect of greatly increased cohesion by local compression of the cometary regolith under the landing pods during landing. Previous relevant regolith modeling work,⁵ and¹² covers both low-velocity (approx. 1 m/s) impact of blunt bodies into dust-rich, fluffy cometary materials (Biele et al⁵), as well as high-velocity (approx. 10 m/s) impact of sharp projectiles on various types of soil. (Allen¹ and Anderson et al²). The lower limit of the tensile strength is of the order of 1kPa whereas the probable upper limit can be taken as 100kPa. The lower limit of tensile strength corresponds to a compressive strength of $c \geq 7\text{kPa}$. This wide range of soil properties must be captured in simulation, which poses a significant challenge.

At very low gravity and vacuum conditions the biggest unknown is the material strength of the surface material. Neither the Deep Impact mission nor other comet observations have provided firm data on the strength of cometary material. Theoretical considerations and laboratory measurements for weakly bound

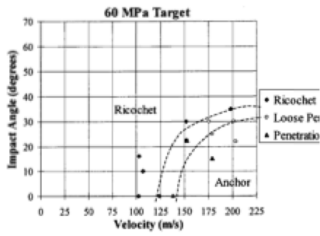


Figure 13. Anchoring Threshold Results for Targets with 60 MPa Compressive Strength

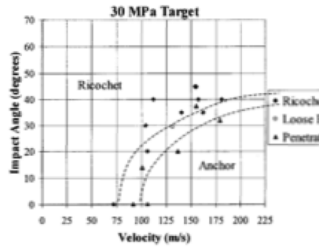


Figure 14. Anchoring Threshold Results for Targets with 30 MPa Compressive Strength

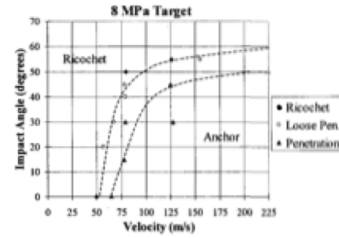


Figure 15. Anchoring Threshold Results for Targets with 8 MPa Compressive Strength

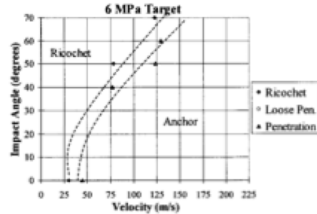


Figure 16. Anchoring Threshold Results for Targets with 6 MPa Compressive Strength

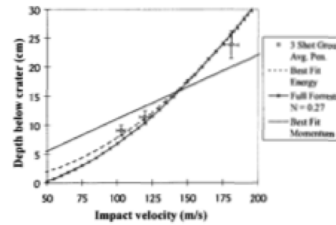


Figure 17. Penetration Depth vs. Impact Velocity

Figure 10. Possibility of Ricochet, taken from²³

aggregates and the few observational constraints available for comets and cometary meteoroids lead to estimates of the quasi-static tensile (or shear) strength of cometary material in the dm to m range as of the order of 1kPa, while the compressive strength is estimated to be of the order of 10kPa. In the following, we summarize the current state of knowledge in asteroidal and cometary regolith behavior.

- *Cohesion, tensile, shear and compressive strength:* While for brittle materials tensile strength is generally less than the shear strength, compressive strength is about one order of magnitude higher than tensile strength. In the case of soft landing compressive strength is the relevant parameter. Shear, tensile and compressive strength are indicated by σ_s , σ_t , σ_c , respectively.
- *Dynamic and quasi-static strength:* During impacts, due to very high strain rates, the dynamic strength is typically higher than the quasi-static strength. It is known that the strength increases with strain-rate resulting in values about an order of magnitude higher (or even more) than the quasi-static strength for the same material. Generally the tensile strength σ_t is proportional to a power b of the strain rate $\dot{\epsilon}$ with a power law exponent typically around 1/4 to 1/3, depending on the material.
- *Size dependence:* Different theories indicate that the strength decreases with increasing size according to d^{-q} where the exponent q is approximately 0.5 (fractal aggregate with fractal dimension $D = 2.5$ of ice). Thus, if extrapolated from typical lander (0.1m), or impactor (1m) to typical comet (1 to 10 km) scales, the size effect alone would produce a factor of 100 in the apparent strengths. This is in line with the observation that comets can often be described as essentially strength-less bodies (large cometary, rubble pile, swarm models) globally, while locally a significant material strength is to be expected.
- *Breakup of Comets, Topography Observations:* Tidal disruption of comets indicate low global tensile strengths in the order of 100 to 10,000 Pa. For example, the break-up of Shoemaker-Levy 9 during its perijove in 1992 set a rough upper limit of the tensile strength (on global/km scales!) of 100Pa. The tensile strength of sun-grazing comets has been estimated as 10kPa with some uncertainty due to thermal stresses. Images by Stardust from comet 81P/Wild-2 showed that the cometary surface must have a finite strength on short scales (< 100 m) to support the observed topographic features; because of the small gravity, some 10Pa might suffice. Otherwise, only lower bounds on the tensile strengths are available in the order of 1 . . . 100 Pa.

- *Breakup of Meteoroids:* Another source of information about possible strength values of cometary surfaces on mm to dm scales stems from the analysis of meteoroids associated with certain comets which enter the earth atmosphere at high speeds and finally break-up and create a light flash. Wetherill²⁶ gives values for tensile strengths of these fireballs ranging from 1 kPa to 1 MPa. More recently, Trigo-Rodríguez and Llorca²⁴ have studied a broad data base of meteor ablation light curves and arrive at tensile strengths between $(400 \pm 100 \text{ Pa}$ and 40 kPa , clustering around 10 kPa for not too evolved and rather low density $< 1 \text{ g/cm}^3$ (if known) cometary meteoroids.
- *Laboratory Measurements:* The small scale (cm) shear and tensile strength of snow in the relevant density range of 300 to 500 kg/m³ is of the order of 10 to 100 kPa. The tensile strength of snow is nearly independent on temperature, while the compressive strength shows a remarkable increase with decreasing temperatures. Simulating possible cometary analogue material in the scope of the KOSI experiments concluded that the small-scale compressive strength of porous mixtures of crystalline ice and dust lies in the range between 30kPa and 1MPa with increasing strength for an increasing dust fraction.
- *Limits Derived from Comet Size and Rotation:* Stability against disruption due to rotation yields lower limits for the combination of bulk density and tensile strength. Rotational periods and sizes for many comets are known, but the corresponding bulk densities are not well constrained. For example, a fast rotating big comet such as C/Hale-Bopp (1995 O1) could be a strength-less rubble pile with a bulk density as low as 100 kg/m³.
- *Theoretical Estimates:* There are different approaches to describe the tensile strength of powders on the basis of van der Waals interactions, cf. Greenberg et al.,⁹ or Chokshi et al.⁷ The latter model includes the elastic deformation of contacting spherical grains. The theoretical tensile strength of fluffy aggregates depends on particle radii, contact areas, packing geometry and typically scales with the bulk density. Greenberg et al. estimate a tensile strength, for interstellar silicate dust/ice material with a density of 280 kg/m³, of 270 Pa. Sirono and Greenberg²² derive 300 Pa for the tensile and 6000 Pa for the compressive strength for a medium composed of ice grains linked into chains by intermolecular forces. Kuhrt and Keller¹⁴ derive a theoretical strength of 100Pa and 100 kPa for grains of 1mm and $1 \mu\text{m}$, respectively. Note that 95% of the Deep Impact ejecta dust cross section is represented by particles $r < 1.4 \mu\text{m}$. From the discussion above the conclusion can be drawn that the cometary surface on meter scales has a reasonable lower limit of the tensile strength of the order of 1kPa whereas the probable upper limit can be taken as 100 kPa.

Now that the foundations of the regolith behavior have been laid out, in the next section we delve into the analysis of the soil interaction process during penetration.

2. Modeling of Forces acting on Penetrating Object

A complete and general solution describing the penetration of a projectile into a solid body is not known, though there are several published models available which may be applicable to the harpoon (see, e.g., those listed by Wang²⁵). For current modeling efforts we consider the harpoon to be a rigid, conically tipped cylindrical projectile, where θ is the half opening angle of the cone.² Several possible forces may contribute to the overall deceleration experienced by the projectile during penetration.¹ These may depend on penetrated depth and velocity as well as target material parameters. Most of the forces can be expressed as the integral of decelerating stresses over the wetted surface S_w of the penetrator in contact with the target material. The main force terms of clear (or plausible) physical origin found in the published literature are as follows:

- A constant term associated with compressive strength, possibly including a contribution from the targets self-weight. The latter should be negligible on the comet, where the surface gravity g is expected to be no more than about 1/2000 of that on Earth. It may be more significant for ground-based experiments where the projectile is fired downwards into a cohesion-less target, though the fact that it is also proportional to the diameter of the projectile means that the term is still quite small for laboratory-scale experiments.
- A term which increases linearly with depth due to the weight per unit volume ρg of the overlying material (overburden pressure). As with the self-weight, this should be negligible on the small body

but needs to be considered for ground-based experiments, especially those with cohesion-less targets. This term is also proportional to a factor $N_q(\phi)$. For the limit $\phi = 0$, $N_q = 1$ and the term becomes analogous to buoyancy in a fluid.

- A dynamic drag term proportional to the target density ρ and the square of velocity V , resulting from the transfer of momentum from the projectile to the target material. In many cases the importance of drag is incorporated by adopting a drag coefficient C_D (which may itself have a velocity dependence), analogous to the parameter used in fluid dynamics.
- Sliding friction between the projectile surface and the target material, governed by the coefficient of sliding friction μ_f and the total normal stress from the three terms above.
- A viscosity or damping term, proportional to the component of velocity parallel to the projectiles surface. As with friction, this force acts parallel to the harpoons surface rather than normal to it. The physical validity of this term seems to be a matter for debate.
- The weight of the projectile. This is only important when significant compared to the other (decelerating forces).

Collecting these terms together with the appropriate geometric factors, one obtains the following equation for the overall deceleration:

$$-\frac{dV}{dt} = \frac{1}{m} \int \int_{S_w} \left[\left(\frac{1}{2} C_D \rho V^2 \sin^2 \theta' + \sigma + \rho g N_q z \right) \times (\sin \theta' + \mu_f \cos \theta') + k_v V \cos^2 \theta' \right] dA - g \quad (17)$$

In this equation, $\theta' = \theta$ along the conical tip, but $\theta' = 0$ along the cylindrical shaft of the penetrating object. Also, from Komle,¹² $N_q(\phi) = \exp(\pi \tan \phi) \tan^2(\frac{\pi}{4} + \frac{\phi}{2})$, and k_v is a constant with units of $[Nsm^{-3}]$, i.e., those of viscosity divided by the thickness of a representative boundary layer around the projectile where viscous flow occurs..

From,¹² a parameter analogous to a drag coefficient can be defined in terms of the material parameters as

$$C_D = \frac{2}{(1-\eta) \cos^2 \theta} \times \left[\frac{(1-\eta) + 1/\alpha + \eta/(2-\alpha)}{\eta^{\alpha/2}} - \frac{1}{\alpha} - \frac{1}{2-\alpha} \right] \quad (18)$$

where $\alpha = 3\lambda/(3+2\lambda)$, $\lambda = \tan(\phi)$, ϕ is the angle of internal friction, $\eta = 1 - \frac{\rho_0}{\rho}$ is the volumetric strain, ρ_0 is the bulk density of the target material before penetration. The case $\eta = 0$ implies zero compression.

After,¹² the compressive stress and the drag term can be combined together, so that the radial pressure exerted on an area element of the target material in contact with an area element of the penetrators surface can be written as:

$$\sigma = [\eta^{-\alpha/2} - 1] \frac{\tau_0}{\lambda} + \left[\frac{(1-\eta) + 1/\alpha + \eta/(2-\alpha)}{\eta^{\alpha/2}} - \frac{1}{\alpha} - \frac{1}{2-\alpha} \right] \frac{\rho_0 V^2 \tan^2 \theta}{(1-\eta)} \quad (19)$$

where τ_0 is the soil cohesion. Note that σ consists of a constant term and a term proportional to the square of velocity, i.e. this model produces neither a term analogous to viscosity nor an overburden pressure term.

The total decelerating force acting on the penetrator consists then of two components. One is the vertical component of the normal stress on the penetrators conical surface, the second being the vertical component of the sliding friction acting tangentially to the projectiles surface. Combining these two components and integrating over the whole wetted surface S_w of the penetrator gives the following expression for the deceleration of the harpoon:

$$-\frac{dV}{dt} = \frac{1}{m} \int \int_{S_w} \left[\left(\frac{1}{2} C_D \rho V^2 \sin^2 \theta' + \sigma + \rho g N_q z \right) \times (\sin \theta' + \mu_f \cos \theta') + k_v V \cos^2 \theta' \right] dA - g \quad (20)$$

To get insight into the sensitivity of the system to the various parameters involved, we derived a simple one-dimensional model of the system behavior during penetration. Assumptions used in the derivation of this reduced model are the following. The harpoon is modeled as a point-like body with variable mass and area. The mass of body increases because of soil compaction. The soil properties are constant. The gravity

level is constant. The soil penetration is modeled following the previous section. The system equations are integrated with a 4-th order constant step Runge-Kutta integrator. Under these assumptions, the final equations of motion of the penetrating harpoon become:

$$v = \dot{h} \quad (21)$$

$$\dot{v} = g - \frac{A\sigma_c}{M} - \frac{\rho AC_D v^2}{2M} \quad (22)$$

$$\dot{m} = \rho A v \quad (23)$$

$$M = m_0 + m(t) \quad (24)$$

$$\sigma_c = s_c c N_c + \rho g \left(\frac{1}{2} s_g A N_g + s_q N_q h \right) \quad (25)$$

where ρ is the soil density, g is the local gravity level, m_0 is the initial mass of the harpoon, σ_c is the maximum soil compressive stress, N_c , N_g , N_q are soil bearing capacity factors, s_c , s_g , s_q are shape factors which depend on the penetrator cross-section shape, and c is the cohesion coefficient. Figure 11, taken from,²¹ depicts the soil bearing stress vs. depth as a function of (a) penetrator mass, and (b) cone angle, confirming the fact that a larger diameter harpoon would penetrate less, and that a heavier harpoon would penetrate deeper. All these results assume an initial approach velocity of 1 m/s.

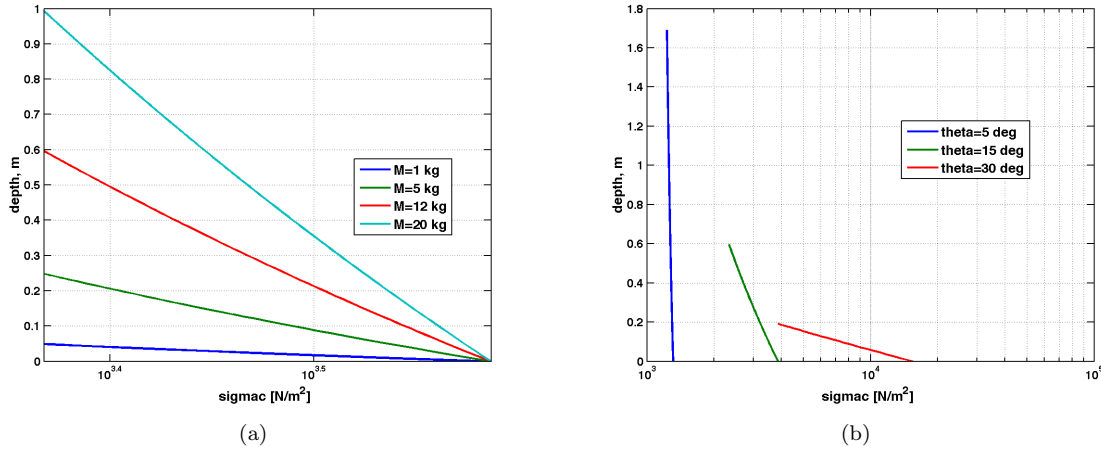


Figure 11. Soil bearing stress vs. depth as a function of (a) penetrator mass, and (b) cone angle.

Now that we have insight into the system behavior with a simple model, we increase the fidelity of the model and consider the soil interaction process with a multibody dynamics model. This is done in the next section.

B. Outgassing and dust ejection models

In this section, we summarize the comet outgassing and dust ejection models. The assumption¹³ is that the comet outgassing field is continuous and it varies from the largest value at the sub-solar point to the minimum value at anti-solar point, and that the outgassing force is radial along the direction \mathbf{u} .⁶ The number of atoms crossing the area A at the distance r from the center of the comet due to time interval δt is given by

$$N = \frac{Q_{gas}(1 + \cos\theta)}{4\pi r^2} A \delta t \quad (26)$$

where Q_{gas} is the gas production rate in molecules per second, θ is the angle between the comet to the sun and the comet to the spacecraft vectors. The total momentum applied to this area is $P_{tot} = 2m_g v_g N$ where v_g is the gas velocity and m_g is the mass of water molecule. The total force on the area is $F_{tot} = P_{tot}/\delta t$.

The pressure field will depend on two variables: angle θ and distance r , and is obtained from the above equations in the form

$$p_{gas} = \frac{\dot{M}_{gas} v_{gas}}{4\pi r^2} (1 + \cos\theta) \quad (27)$$

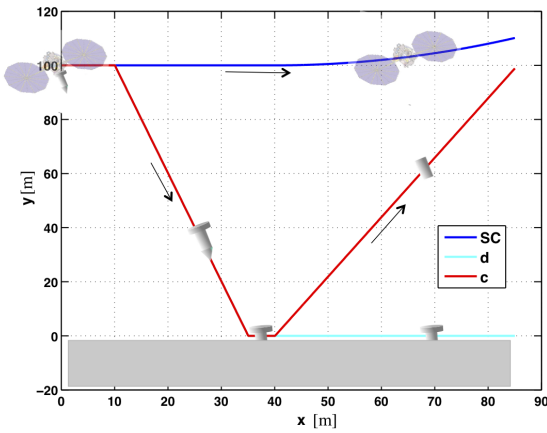
where $\dot{M}_{gas} = m_{gas} Q_{gas}$ is the gas mass loss rate. Consequently, the gas (outgassing or dust) induced acceleration on the spacecraft can be computed as:

$$\mathbf{a}_{gas} = \frac{p_{gas} A_{sc} \mathbf{u}}{m_{sc}} (1 + \cos\theta) \quad (28)$$

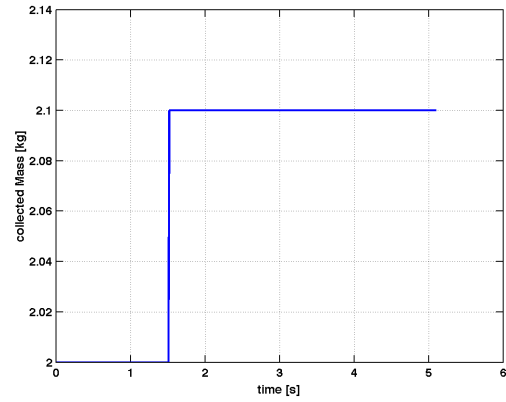
Following,¹³ the parameters used in the outgassing model are): water production rate $Q_{gas} = 3 \times 10^{28}$ (molecules/sec), gas loss rate $\dot{M}_{gas} = 300$ (kg/sec), gas ejection velocity $v_{gas} = 600$ (m/sec), and the parameters of dust ejection model are: dust mass distribution m_{dust} from 10^{12} to 10^7 (kg), min/max dust size d from 2×10^5 to 8×10^3 (m), dust ejection velocity $v_{dust} = 300$ (m/sec), dust mass loss rate $\dot{M}_{dust} = 100$ (kg/sec).

V. Simulation Results of System with Harpoon and no Tether

In this section, we discuss the results of the simulation study. Figure 12 (a) shows a simulation snapshot of the scenario with no tether. Note that the harpoon would remain emplaced in the ground, while the canister would fly back towards the spacecraft, which would be accelerating away under the thrust. Figure 12 (b), shows the amount of material that would be collected inside the canister, as a result of the ground penetration event. Figure 13 shows the spacecraft position (a), velocity (b), acceleration (c), quaternion (d) angular velocity (e), angular acceleration (f) during the mission event. Note the acceleration step at 2.5 seconds, indicating the fly-away thrusting event. Figure 14 shows the harpoon position (a), velocity (b), acceleration (c), quaternion (d) angular velocity (e), angular acceleration (f) during the mission event. Notice the the first spike of acceleration at the moment of ground penetration (approx. 1 second), and the second spike of angular acceleration at 2.5 seconds when the canister is ejected from the harpoon. Figure 15 shows the canister position (a), velocity (b), acceleration (c), quaternion (d) angular velocity (e), angular acceleration (f) during the mission event. Notice the the first spike of angular acceleration at the moment of ground penetration (approx. 1 second), and the second spike of linear acceleration at 2.5 seconds when the canister is ejected from the harpoon. Figure 16 shows the components of the relative distance between the spacecraft and the container, confirming that the container would be recovered successfully by reaching the spacecraft once it has been ejected. Figure 17 shows the simulated (a) soil penetration force, and (b) the soil penetration torque, while Figure 18 shows the (a) soil penetration depth, and (b) the soil penetration depth rate. Figure 19 shows the soil compressive strength as a function of time. Finally, Figures 20, 21, and 22 show the solar pressure, comet dust, and comet outgassing forces and torques, during the event. The magnitude of these forces is very small, consistent with the results presented in⁵ and in Figure 8.

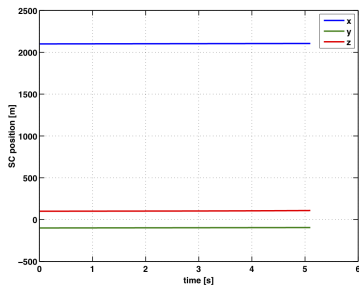


(a)

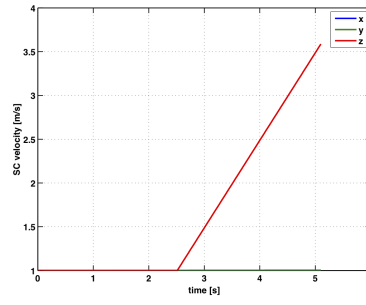


(b)

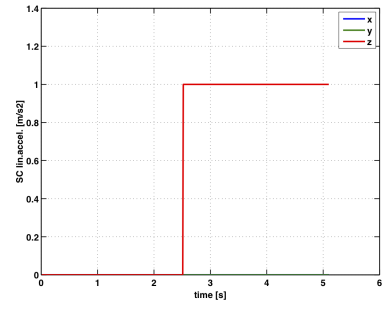
Figure 12. (a) Simulation snapshot: no tether, and (b) Container mass.



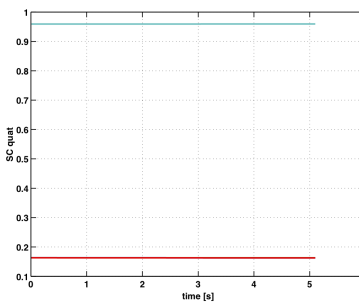
(a)



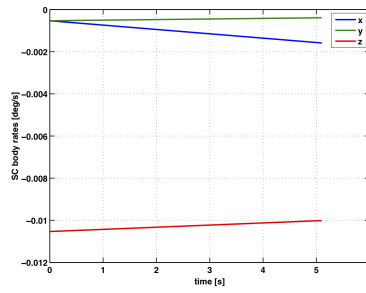
(b)



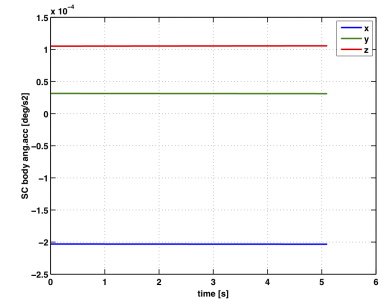
(c)



(d)



(e)



(f)

Figure 13. Spacecraft position (a), velocity (b), acceleration (c), quaternion (d) angular velocity (e), angular acceleration (f).

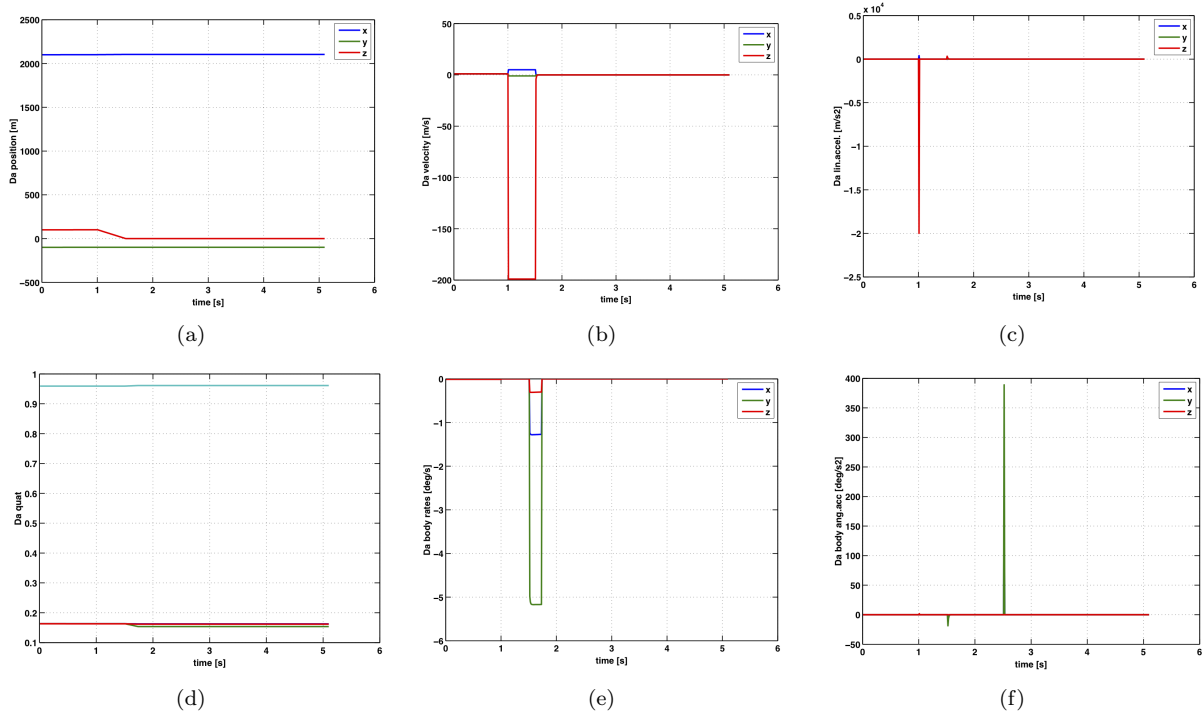


Figure 14. Harpoon position (a), velocity (b), acceleration (c), quaternion (d) angular velocity (e), angular acceleration (f).

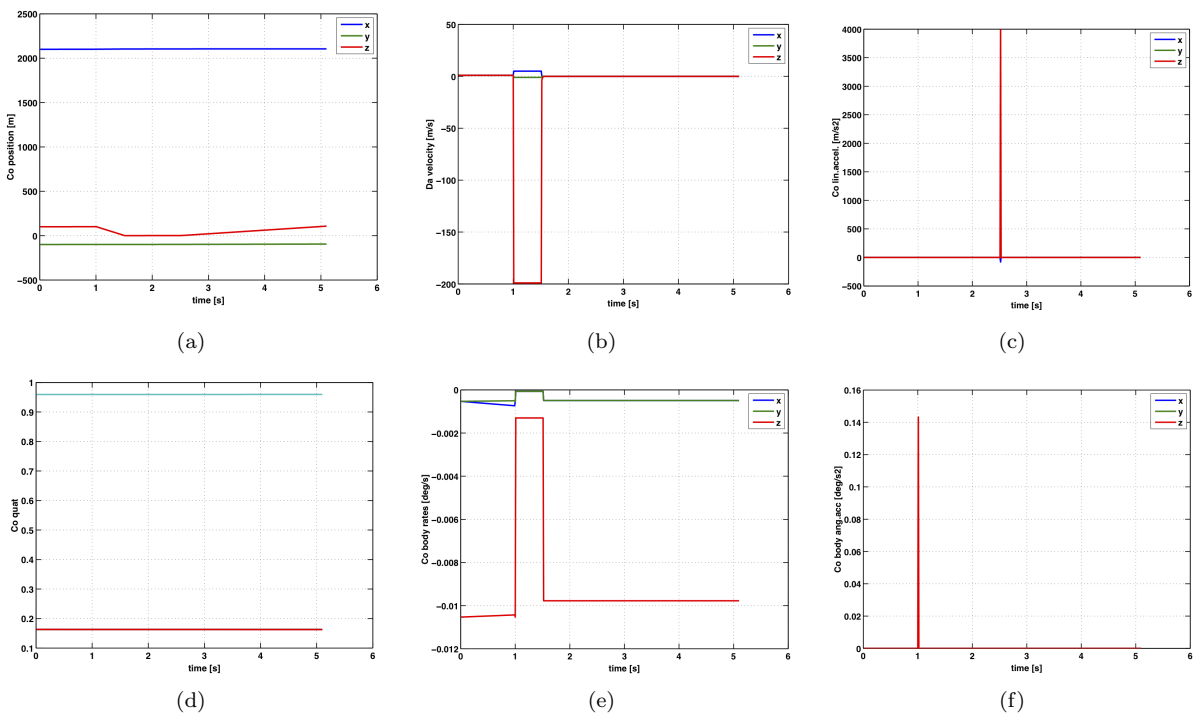


Figure 15. Container position (a), velocity (b), acceleration (c), quaternion (d) angular velocity (e), angular acceleration (f).

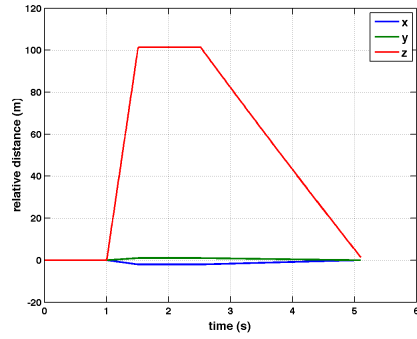
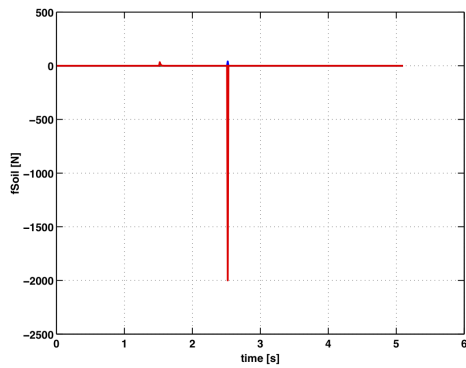
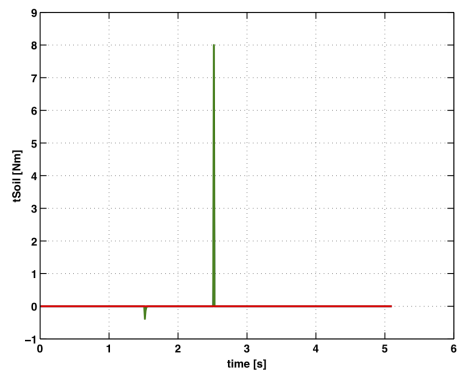


Figure 16. Relative distance between spacecraft and container

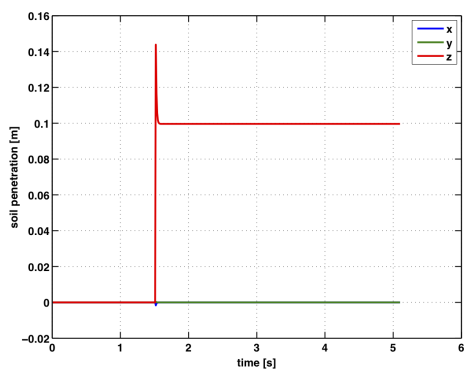


(a)

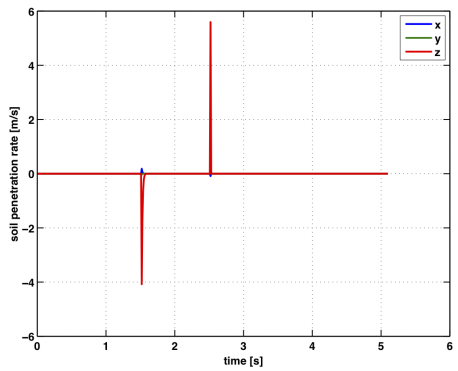


(b)

Figure 17. (a) Soil Penetration Force, and (b) Soil Penetration Torque.



(a)



(b)

Figure 18. (a) Soil Penetration Depth, and (b) Soil Penetration Depth Rate.

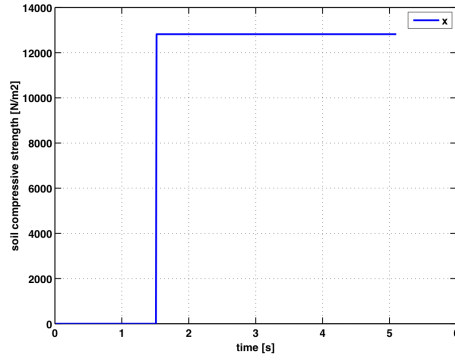
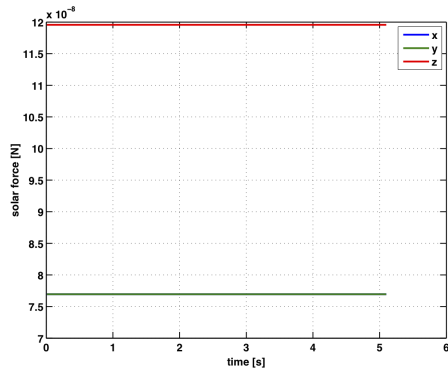
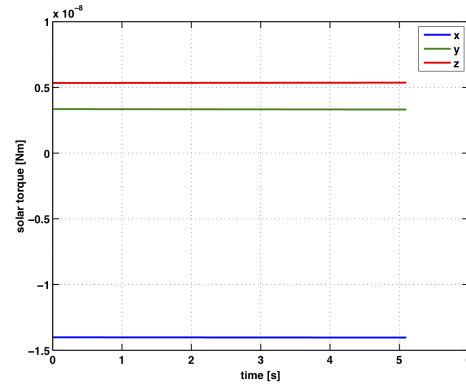


Figure 19. Soil Compressive Strength

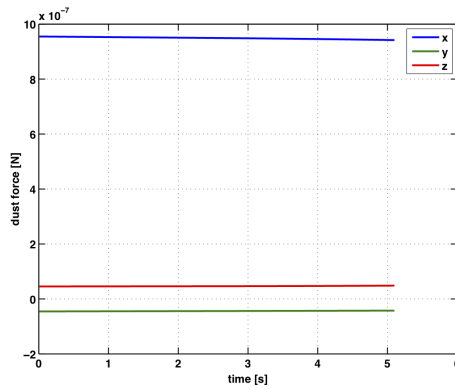


(a)

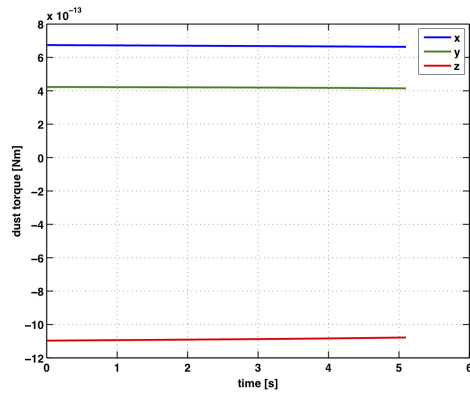


(b)

Figure 20. (a) Solar Pressure Force, and (b) Solar Pressure Torque.

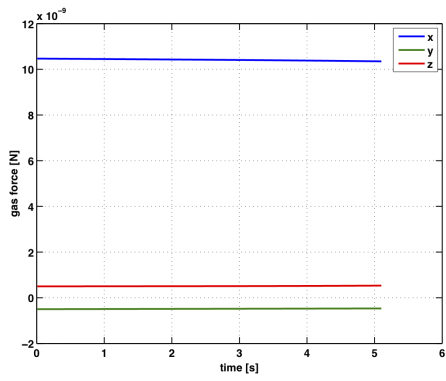


(a)

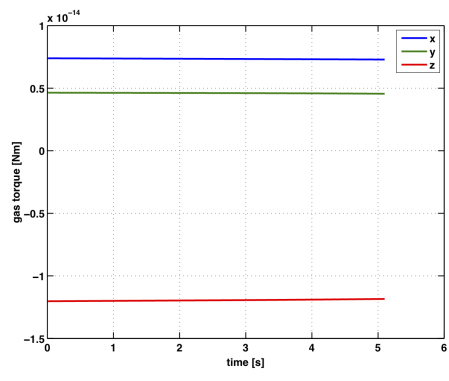


(b)

Figure 21. (a) Comet Dust Force, and (b) Comet Dust Torque.



(a)



(b)

Figure 22. (a) Comet Outgas Force, and (b) Comet Outgas Torque.

VI. Simulation Results of Tether-Assisted Retrieval of Harpoon

In this section, we discuss the effect of adding a tether to retrieve the canister. Figure 5 summarizes the various system parameters considered in this study. The pictorial depiction of the model and the parameters used in the simulation are shown in Figure 23 (a). A viscoelastic spring-dashpot is used to model the tether, connecting the harpoon to the spacecraft. For simplicity, the problem is two-dimensional. At the initial conditions, the system is hovering along the radial direction, with the canister on the ground at zero velocity (just released from the harpoon casing), while the spacecraft is at 100 meter altitude and has velocity initial conditions both in the vertical and the horizontal directions. These velocity initial conditions represent initial dispersions in velocity accounting for control imperfections. Figure 23 (b) shows the timeline and a snapshot of the tethered harpoon leaving the surface as the spacecraft pulls it. A 0.1 N-s ejection impulse from the surface is applied to the Canister at 0 sec. Spacecraft fly-away acceleration (thrusting) is initiated at 0.2 s, and tether retrieval is initiated after 5 seconds. The assumed Isp for the spacecraft fly-away thrusters is 220 s.

Figure 24 shows the trajectory of system from initial condition, bringing into evidence the system transfer of angular momentum which takes place the moment the canister is released from the harpoon. Figure 25 shows (a) the tether tension upon retrieval, and (b) the tether stretch upon retrieval. Figure 26 shows (a) the tether strain upon retrieval, and (b) the tether Length upon retrieval. Figure 27 shows (a) the tether length rate upon retrieval, (b) the tether length as a function of tether retrieval rate, and (c) the system rotational speed upon retrieval.

The results of the sensitivity study as the fly-away thrust varies from 10 to 30 N, are summarized in Figure 28. These results indicate that the tether retrieval is achievable with reasonable dV fuel budget, and that the tether pendulum mode angle amplitude angle is smaller with larger thrust.

Figure 28 also shows the sensitivity as a function of increasing the horizontal velocity dispersion from 1 to 10 cm/s, which increases both canister swing angle and tether tension. This case was important to analyze because the canister swing angle was bounded to stay within the camera FOV for visual tracking, especially at close distances.

Figure 29 shows the sensitivity as the initial vertical dispersion velocity is varied from 1 to 3 m/s, and shows that, except for the initial transient, the tether pendulum model amplitude angle is insensitive to vertical velocity dispersion. Figure 29 also show the sensitivity as the tether retrieval rate is varied from 10 to 30 cm/s, and shows that the canister angle is practically insensitive to tether retrieval rate.

The tether pendulum motion could potentially be reduced with a S/C pendulum cancellation maneuver using well-established techniques of vibration reduction using input shaping. This maneuver would track the canister motion, e.g. visually, and the spacecraft would execute lateral motion to reduce overall tether pendulum angle, repeating the cancellation motion to further reduce pendulum angle.

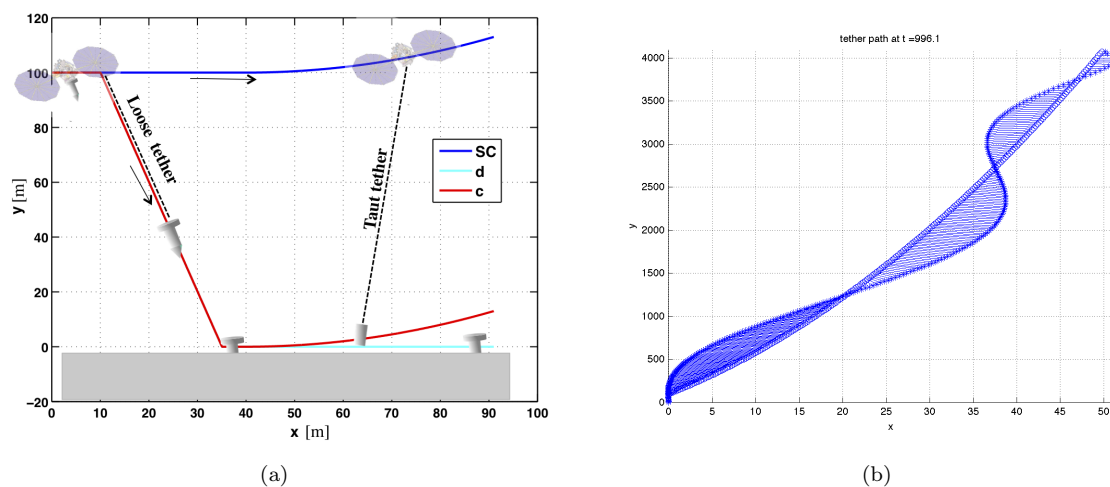


Figure 23. (a) Simulation snapshot: with tether, and (b) trajectory during tether retrieval.

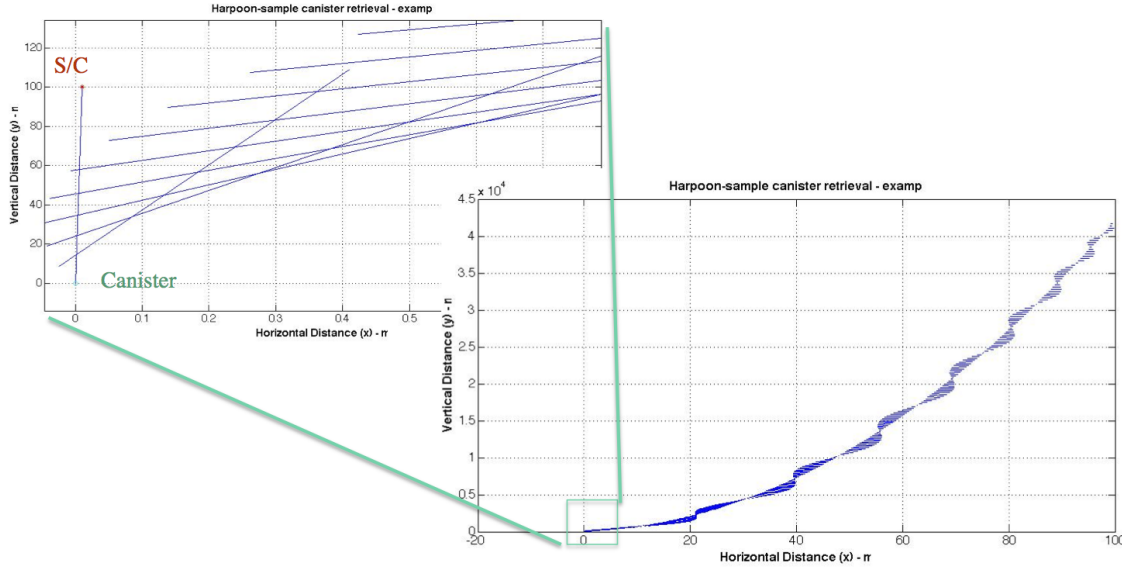
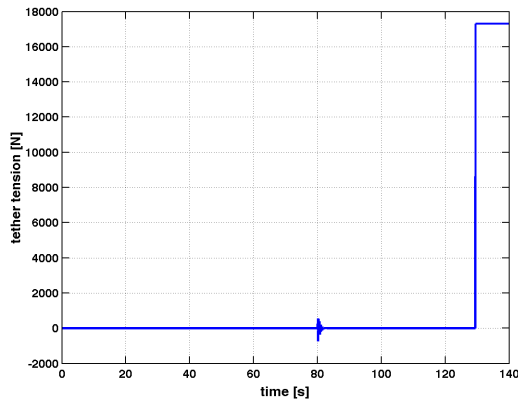


Figure 24. Trajectory of system from initial condition.

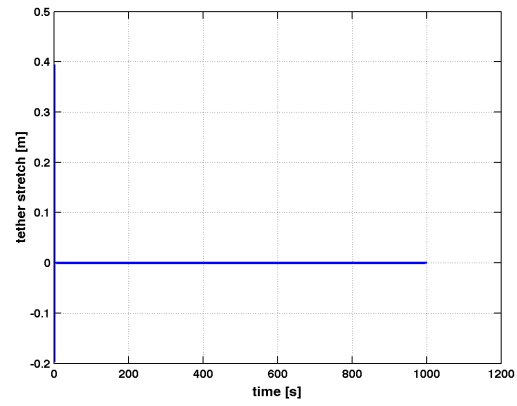
VII. Conclusions

This paper described the development of a dynamic model and simulation results of a tethered and untethered harpoon for comet sampling. This model and simulation was done in order to carry out an initial sensitivity analysis for key design parameters of the tethered system. The harpoon contains a canister which collects a sample of soil from the cometary surface. Both a spring ejected canister and a tethered canister are considered. To arrive in close proximity of the spacecraft at the end of its trajectory so it can be captured, the free-flying canister needs to be ejected at the right time and with the proper impulse, while the tethered canister must be recovered by properly retrieving the tether at a rate that avoids an excessive amplitude of oscillatory behavior during the retrieval. Then results of the simulation with our a tether indicate that the canister can get within reach of the spacecraft so it can be captured, and that the comet environmental forces have negligible magnitude to affect its trajectory. A tether-coupled spacecraft-canister system was modeled and simulated. Specifically, the simulation model consists of a tethered spacecraft (point mass), and a canister-sampler (point mass) connected to the spacecraft by a tether. The tensile force between these bodies is governed by a linear elastic spring model. The contact force with the ground is modeled by a nonlinear soil-interaction model. Both the spacecraft trajectory and the tether-length trajectory are coordinated in a manner that ensures that the relative velocity between the spacecraft and the sampler (tethered harpoon) approaches zero at rendezvous (i.e. the sampler capture event). A sensitivity analysis for key design parameters of tethered and untethered system was conducted, showing that: a) the tether retrieval would be achievable with reasonable spacecraft fuel budget; b) the tether pendulum mode angle amplitude angle would become smaller with increasing spacecraft thrust, and c) the tether pendulum model amplitude angle would be insensitive to tether retrieval rate.

Acknowledgement The research described in this paper was carried out at the Jet Propulsion Laboratory, California Institute of Technology, under a contract with the National Aeronautics and Space Administration. The author is very grateful to Mr. Asif Ahmed for the direction of the task and for challenging the author to think out of the box.

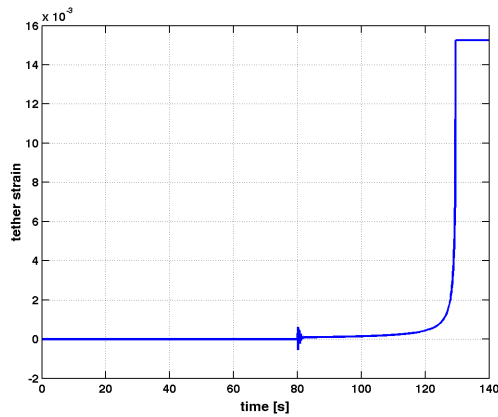


(a)

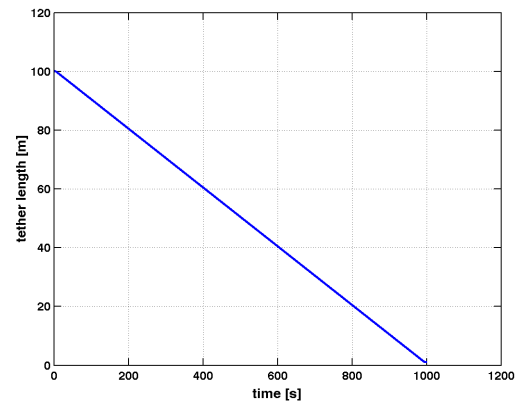


(b)

Figure 25. (a) Tether tension upon retrieval, and (b) Tether stretch upon retrieval.



(a)



(b)

Figure 26. (a) Tether strain upon retrieval, and (b) Tether Length upon retrieval.

References

¹Allen, W.A., Mayfield, E.B., Morrison, H.L., "Dynamics of a projectile penetrating sand". J. Appl. Phys. 28 (3), 1957, 370376.

²Anderson, W.W., Ahrens, T.J., Gibson, A., Scott, R., Suzuki, K., "Emplacement of penetrators into planetary surfaces". J. Geophys. Res. 101 (E9), 21,1996, 13721,149.

³Backes, P., J. Jones, and C. Gritters, Harpoon-based Sampling for Planetary Applications, presented at the IEEE Aerospace Conference, Big Sky, MT, March 2008.

⁴Balaram, J., Cameron, J., Jain, A., Kline, H., Lim, C., Mazhar, H., Myint, S., Nayar, H., Patton, R., Pomerantz, M., Quadrelli, M., Shakkotai, P., Tso, K.: Physics-based Simulator for NEO Exploration: Analysis and Modeling, presented at the AIAA SPACE 2011 Conference and Exposition, Long Beach, California, 14-17 September 2011.

⁵Biele et al., The putative mechanical strength of comet surface material applied to landing on a comet, Acta Astronautica 65 (2009) 11681178.

⁶M. Fille, J.F. Clifo and A.V. Rodionov, Numerical simulation of the dust flux on a spacecraft in orbit around an aspherical cometary nucleus-1, Astronomy and Astrophysics 347(1999) 1009.

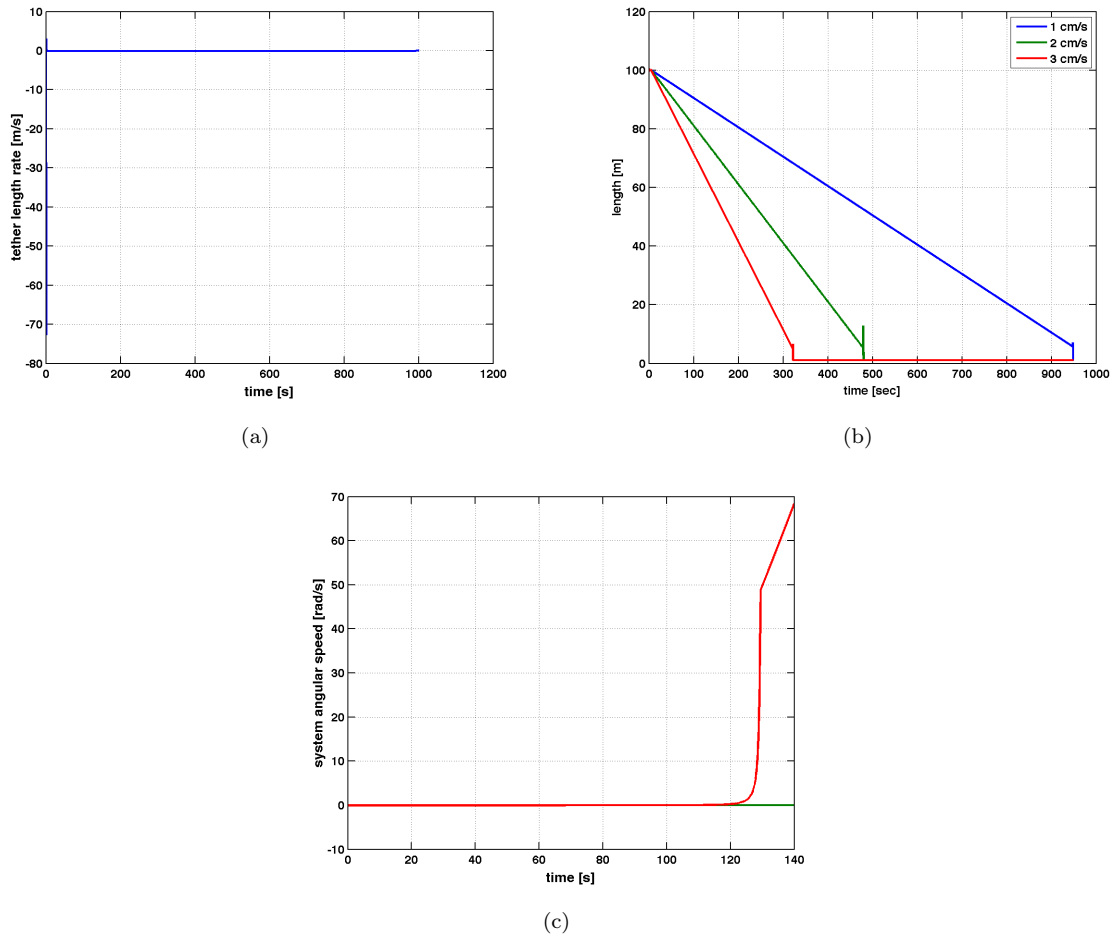


Figure 27. (a) Tether length rate upon retrieval, (b) Tether length as a function of tether retrieval rate, and (c) System rotational speed upon retrieval.

⁷Finzi, A.E., F.B. Zazzera, C. Dainese, F. Malnati, P.G. Magnani, E. Re, P. Bologna, S. Espinasse, and A. Olivieri, SD2 How to Sample A Comet, Space Science Reviews 128(14): 281299, 2007.

⁸Glassmeier, K. et. al., The Rosetta Mission: Flying Towards the Origin of the Solar System, Space Science Reviews 128(14): 121, October 2006.

⁹J.M. Greenberg, H. Mizutani, T. Yamamoto, A new derivation of the tensile strength of cometary nuclei: application to Comet ShoemakerLevy 9, Astron. Astrophys. 295 (1995) L35L38.

¹⁰Haug, E.J.: *Computer-Aided Kinematics and Dynamics of Mechanical Systems, Volume I: Basic Methods*, Allyn and Bacon, Needham Heights, Massachusetts, 1989.

¹¹Kaufman, R., Comet Harpoon Being Test Fired in NASA Lab, National Geographic Daily News, December 13, 2011, available at: <http://news.nationalgeographic.com/news/2011/12/111215-nasa-comet-harpoon-sample-crossbow-space-science/>.

¹²N.I. Komle et al., Impact penetrometry on a comet nucleus interpretation of laboratory data using penetration models, Planetary and Space Science 49 (2001) 575598.

¹³Kulikov, I., JPL Internal Document JPL D-32945, September 23, 2005.

¹⁴E. Khrt, H.U. Keller, The formation of cometary surface crusts, Icarus 109 (1994) 121132.

¹⁵Beletskii, V.V., and Levin, E.: Dynamics of Space Tether Systems, vol. 83 of the Advances in the Astronautical Sciences, 1993.

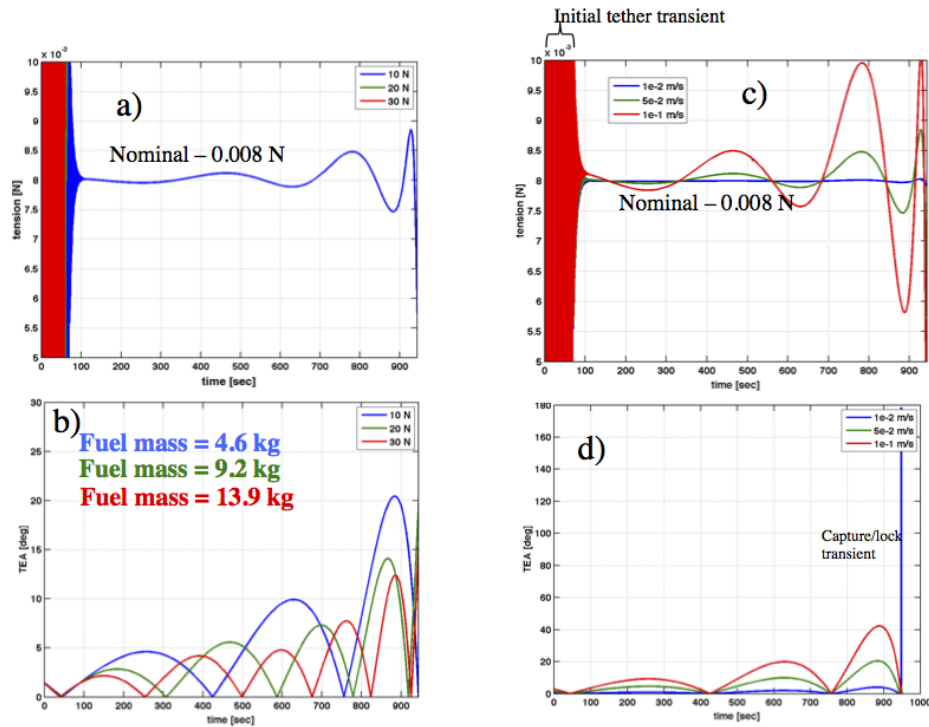


Figure 28. (a) Tether tension and (b) tether angle varying thrust from 10 to 20 N. (c) Tether tension and (d) tether angle varying the horizontal velocity dispersion from 0.01 to 0.1 m/s.

¹⁶Lorenz, R., W. Boynton, and C. Turner, Demonstration of Comet Sample Collection by Penetrator, in Proceedings of the 5th IAA International Conference on Low-Cost Planetary Missions, Noordwijk, The Netherlands, September 24-26, 2003.

¹⁷Lorenz, R., Planetary Penetrators: Their Origins, History, and Future, *Advances in Space Research* 48(3): 403431, August 2011.

¹⁸Matunaga, S., Masumoto, S., Yamanaka, T., Mori O. and Nakaya, K.: Retrieving Dynamics and Control of Tethered Sampling Method for Minor Body Exploration, paper AIAA 2006-6763, presented at AIAA/AAS Astrodynamics Specialist Conference and Exhibit 21 - 24 August 2006, Keystone, Colorado.

¹⁹Matunaga, S., Yamanaka, T., Ashida, H., Nishida, J., Nakaya, K. and Mori O.: Microgravity Experiment of Reel Mechanism for Tethered Sampling, *Space Utiliz Res*, 23 (2007).

²⁰Quadrelli, B.M., Backes, P., Wilkie, W.K., Keim, J., Quijano, U., Mukherjee, R., Scharf, D., Bradford, S.C., McKee, M.: Investigation of Phase Transition-Based Tethered Systems for Small Body Sample Capture, *Acta Astronautica*, 68, (2011), 947-973.

²¹Quadrelli, M., Mazhar, H., Negrut, D.: Modeling and Simulation of harpooning Processes for Small Body Exploration, AIAA SPACE 2012 paper. AIAA2012-5310.

²²S.-I. Sirono, J.M. Greenberg, Do cometesimal collisions lead to bound rubble piles or to aggregates held together by gravity?, *Icarus* 145 (2000) 230238.

²³Stelzner and Nasif, harpooning Technology for in-situ Exploration of Small Bodies, IEEE paper 0-7803-5846-5, 2000.

²⁴J.M. Trigo-Rodriguez, J. Llorca, The strength of Cometary meteoroids: clues to the structure and evolution of comets, *Mon. Not. R. Astron. Soc.* 372 (2006) 655660 erratum (375 (2006) 415415).

²⁵Wang, W.L.: "Low velocity projectile penetration". *J. Soil Mech. Found. Div. Proc. Am. Soc. Civ. Engrs* 97 (SM12), 1971, 16351655.

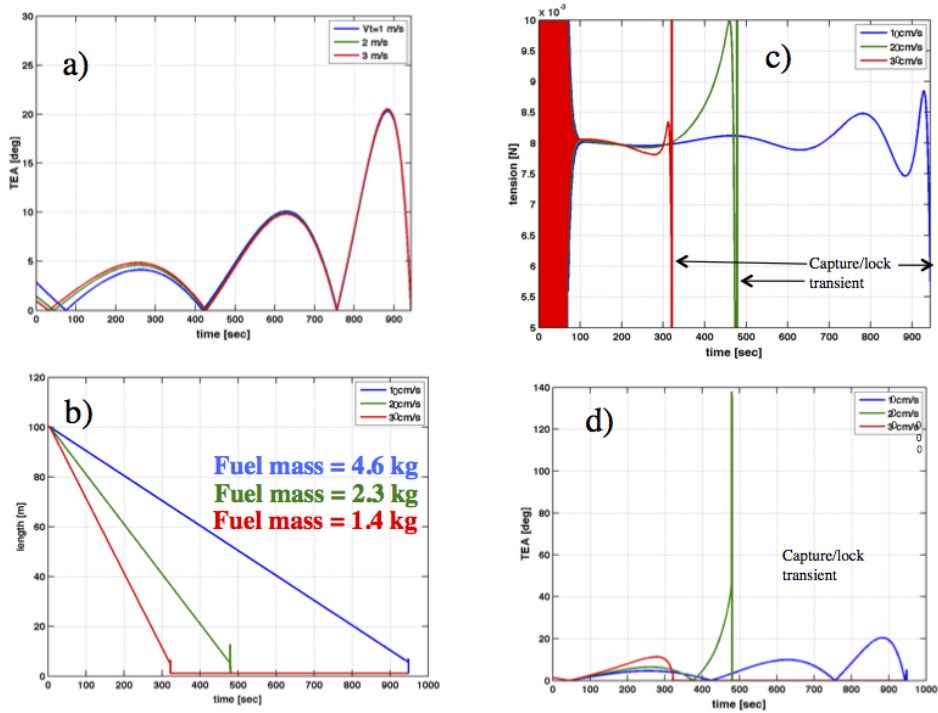


Figure 29. (a) Tether tension and (b) tether angle varying vertical velocity dispersion from 1 to 3 m/s. (c) Tether tension and (d) tether angle varying tether retrieval speed from 10 to 30 cm/s.

²⁶G.W. Wetherill, D.O. Revelle, Relationships between comets, large meteors, and meteorites, in: Comets, University of Arizona, Tucson, AZ, 1982, pp. 297319.

²⁷Wong, J.: Analysis of Tethers in Sampling Near Earth Objects, Air Force Institute of Technology M.S. Thesis, 1997.

²⁸Yano, H., Sampling Systems for Hayabusa and Follow-on Missions: Scientific Rationale, Operational Considerations, and Technological Challenges, presented at the International Marco Polo Symposium and Other Small Body Sample Return Missions, Paris, France, May 1820, 2009.